Iranian Journal of Science and Technology, Transactions of Mechanical Engineering (2021) 45:1115–1122
https://doi.org/10.1007/s40997-019-00339-3

RESEARCH PAPER

Deriving Approximate Criteria for Design and Analysis of a Novel Oscillatory Wind Turbine Using Linearization

Radmarz Hosseinie[1]

Received: 14 June 2019 / Accepted: 27 November 2019 / Published online: 12 December 2019

Abstract
Wind energy has become one of the most popular resources of clean energy. In spite of this popularity, there are some serious flaws in design of conventional wind turbines. Among these are the substantial limitations and drawbacks of the rotary wind turbines, which are the main industrial wind turbines. This has motivated alternative designs and strategies for wind harvesting. In this paper, an alternative oscillatory wind turbine is investigated. First, the governing equations of motion of the turbine are represented and linearized. Then, closed solutions of the linearized equations are cross-validated with numerical simulation resulted from a generated computer code. A close affinity has been observed between the numerical simulation and the analytical solution. Finally, some parametric relationships are extracted from the linearized equations of motion, to be used in design and analysis of the turbine, at least approximately. For validating the utilized method, the C_P of the turbine is derived and compared with the results of numerical simulation. Comparison shows acceptable capability of the method to forecast the behavior of turbine and consequently, its suitability for use as a method for deriving approximate design criteria.

Keywords Oscillatory wind turbine · Equations of motion · Linearization · Design criteria

1 Introduction

The gradual development of the so-called "sustainable engineering" necessitates the replacement of fossil resources of energy with clean and perpetual ones. One of the main resources of clean energy is the wind energy.

Wind energy is becoming more popular all around the world (EWEA 2017; AWEA 2017). There are several designs for wind turbine, among which some have become commercialized and have been utilized in wind farms, such as horizontal axis wind turbines, which are the most common industrial types.

In the past few decades, the concept of oscillating hydro turbines has become a reality, and their relatively high efficiency (about 28% (McKinney and DeLaurier 1981), 34% (Kinsey and Dumas 2008) and even up to 87% for propulsive efficiency (Anderson et al. 1998)) has attracted the attention of many researchers. Platzer et al. (2008), Xiao and Zhu (2014), Young et al. (2014), and Bakhshandeh Rostami and Armandei (2017) provided extensive reviews of almost 40 years of progress in the field of oscillating wing turbines.

The concept of oscillating wing was introduced by McKinney and DeLauriert (EWEA 2017). After McKinney and DeLauriert, work on the oscillating wing has continued till now by many authors, investigating different design aspects, the behavior of fluid field, in addition to searching for optimum performance conditions.

The motion of the oscillating wing is mainly plunging in combination with pitching. Since this combinational motion of oscillating wing is inspired by flapping of swimming and flying animals, the oscillating wing is essentially known as a biomimetic design [see for example Lan (1979), Triantafyllou et al. (2000) and Liu et al. (2012)].

In this work, an innovative design for oscillating wind turbine is proposed and studied. This biomimetic wind turbine sways against the wind, similar to the plants. It is hoped that the method of harvesting power from the wind utilized in this new design will overcome the limitations and drawbacks of the rotary wind turbines and can be employed as an alternative for the conventional rotary ones.

For development in design and better analysis of this turbine, the parametric relationships and criteria are extremely useful, even if they are approximate, to be used as a preferred

✉ Radmarz Hosseinie
hosseini.r@fasau.ac.ir

[1] Fasa University, Fasa, Iran

approach. The equations of motion of this turbine are nonlinear and conditional. Therefore, it is very hard, if not impossible, to study the behavior of the turbine analytically.

One of the popular ways to analytically study nonlinear dynamical systems is to linearize the equations of motion around their equilibrium states (Arrowsmith and Place 1995; Perko 1991). Here, to extract approximate parametric relationships and criteria, the governing equations of motion of the turbine are linearized. These linearized equations, if validated by numerical simulations and experimental data, can be utilized to extract approximate parametric relationships.

It is noteworthy that for simplicity of calculations and due to the goal of this work which is deriving approximate criteria for design and analysis of the proposed turbine, as a suitable approach, a reduced dynamics of the turbine is approximated neglecting the sail dynamics (see Sect. 2.3).

In this paper, the physical configuration and the equations of motion of the proposed turbine are represented. The equations of motion of the wind turbine are linearized around their equilibrium state.

For validating the linearized equations of motion, a computer code is generated in MATLAB to solve the equations of motion numerically.

The linearized equations of motion and the computer code have both been fed with a similar set of benchmark parameters. The closed solution of linearized equations of motion and the results of numerical simulation show good likelihood.

Eventually, some relationships have been extracted from the linearized equations of motion to be used as approximate design and analysis criteria. Also, an approximate formula for C_P is derived and validated.

2 The Governing Equations of Motion of the Turbine and their Linearized Form

Figure 1 shows the configuration of the proposed wind turbine, schematically. Although this turbine is supposed to generate electrical power, in this study, we simply consider a belt-type dynamometer to put constant resistive torque on the flywheel of the turbine.

2.1 Physical Configuration of the Turbine

According to Fig. 1, the proposed turbine is comprised of a sail which is hinged to the top of a mast. The mast is hinged on a base and can oscillate. A rotational spring is attached to the axis of the mast, and a flywheel is mounted on this axis.

The sail is equipped with a switching mechanism which rotates the sail between vertical and inclined orientations periodically, in a certain period of time. For measuring the harvested wind power, a belt dynamometer harnesses the flywheel by generating friction torque. A ratchet mechanism rectifies the rotation of flywheel.

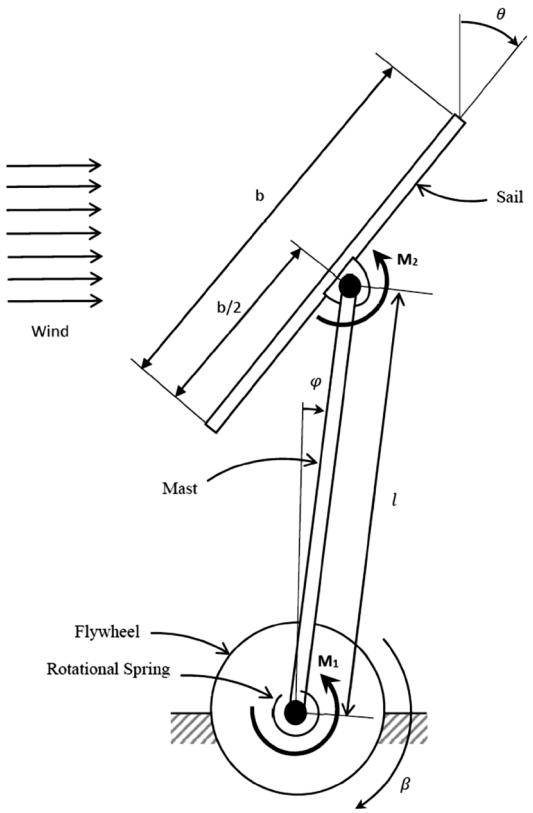

Fig. 1 Configuration of the turbine

When the sail is vertical, the wind exerts maximum drag on the sail, and the mast pushes the flywheel, and consequently, the wind power is extracted. This is the coupled phase of the motion of turbine. When the sail switches to an angle drifted from the vertical direction, the drag on the sail reduces and the spring returns the mast. The mast therefore detaches from the flywheel due to the ratchet mechanism. This is the decoupled phase of motion. The turbine will therefore continuously oscillate, and the wind energy will be harvested.

2.2 The Turbine Equations of Motion

Assuming the wind to be steady, uniform and horizontal, the equation of rotation of the sail is

$$\bar{I}_2\ddot{\theta} = e(F_{\mathrm{D}}\sin\theta + F_{\mathrm{L}}\cos\theta) + M_2, \tag{1}$$

where θ is the angle of sail with respect to the vertical direction, M_2 is the moment exerted by the switching mechanism on the sail, e is the position of center of pressure with respect to the axis of rotation, I_2 is the sail inertia, and F_{D} and F_{L} are drag (horizontal) and lift (vertical) components of aerodynamic force exerted on the sail.

The equations of motion for decoupled phase are

$$\left(\bar{I}_1 + m_1 r^2 + m_2 l^2\right)\ddot{\varphi} + K_1\varphi - \left(m_1 r + m_2 l\right)g\sin\varphi = l(F_{\mathrm{D}}\cos\varphi + F_{\mathrm{L}}\sin\varphi) - M_2, \tag{2}$$

and

$$J\ddot{\beta} = T_{\text{resistive}}, \tag{3}$$

where $\bar{I}_1$ is the mast inertia around its center of mass, m_1 is the mass of mast, m_2 is the mass of sail, l is the length of the mast, r is the position of center of mass of the mast with respect to its center of rotation, K_1 is the stiffness of the rotational spring, φ is the angle of mast with respect to the vertical direction, and β is the angle of flywheel.

The dynamometer torque is represented by $T_{\text{resistive}}$, which is modeled by Coulomb dry friction (Armstrong-Helouvry et al. 1994; Pennestri et al. 2016):

$$T_{\text{resistive}} = \begin{cases} -T_{\text{kinetic frcition}}\operatorname{sgn}\left(\dot{\beta}\right) & \text{if } \dot{\beta} \neq 0 \\ 0 & \text{if } \dot{\beta} = 0 \end{cases}, \tag{4}$$

where $T_{\text{kinetic frcition}}$ is the kinetic friction torque between dynamometer and flywheel.

The equation of motion of the coupled phase is

$$\left(\bar{I}_1 + m_1 r^2 + m_2 l^2 + J\right)\ddot{\varphi} + K_1\varphi - \left(m_1 r + m_2 l\right)g\sin\varphi = l(F_{\mathrm{D}}\cos\varphi + F_{\mathrm{L}}\sin\varphi) - M_2 + T_{\text{resistive}}, \tag{5}$$

where J is the inertia of the flywheel. Using Karnopp model for sticking and sliding phenomena in dry friction (Pennestri et al. 2016):

$$T_{\text{resistive}} = \begin{cases} -\min\left(\max\left(T_{\text{static}} - T_{\text{static friction}}\right)\cdot T_{\text{static friction}}\right) & \text{if } \dot{\varphi} = 0 \\ -T_{\text{kinetic friction}}\operatorname{sgn}(\dot{\varphi}) & \text{if } \dot{\varphi} \neq 0 \end{cases}, \tag{6}$$

where T_{static} is the torque exerted by the mast on the flywheel if the turbine is stationary:

$$T_{\text{static}} = -K_1\varphi + \left(m_1 r + m_2 l\right)g\sin\varphi + l(F_{\mathrm{D}}\cos\varphi + F_{\mathrm{L}}\sin\varphi) + M_2, \tag{7}$$

and $T_{\text{static friction}}$ is the static friction torque, which is used as a threshold for the onset of sliding.

The drag and lift components of aerodynamic force are

$$F_{\mathrm{D}} = \frac{1}{2}C_{\mathrm{D}}\rho_{\text{air}}AV_{\text{rel}}^2, \tag{8}$$

and

$$F_{\mathrm{L}} = \frac{1}{2}C_{\mathrm{L}}\rho_{\text{air}}AV_{\text{rel}}^2, \tag{9}$$

where $C_{\mathrm{D}} = C_{\mathrm{D}}(\theta\cdot\mathrm{AR})$ and $C_{\mathrm{L}} = C_{\mathrm{L}}(\theta\cdot\mathrm{AR})$ are drag and lift coefficients, respectively, in which AR is the aspect ratio of the sail, A is the area of the sail, and

$$V_{\text{rel}} = U - l\dot{\varphi}\cos\varphi, \tag{10}$$

where U is the wind speed.

2.3 Linearization of the Equations of Motion

Assume $\bar{\varphi}$ is the equilibrium angle where the mast oscillates around and $\tilde{\varphi}$ is the small amplitude of oscillations of the mast around $\bar{\varphi}$. Therefore $\varphi = \tilde{\varphi} + \bar{\varphi}$.

First, we linearize the aerodynamic force components:

$$V_{\text{rel}} = U - l\dot{\tilde{\varphi}}\cos\tilde{\varphi}\cos\bar{\varphi} + l\dot{\tilde{\varphi}}\sin\tilde{\varphi}\sin\bar{\varphi} \simeq U - l\dot{\tilde{\varphi}}\cos\bar{\varphi}. \tag{11}$$

Substituting in Eqs. (8) and (9), we have

$$F_{\mathrm{D}} \simeq \frac{1}{2}C_{\mathrm{D}}\rho_{\text{air}}A\left(U^2 - 2Ul\dot{\tilde{\varphi}}\cos\bar{\varphi}\right), \tag{12}$$

and

$$F_{\mathrm{L}} \simeq \frac{1}{2}C_L\rho_{\text{air}}A\left(U^2 - 2Ul\dot{\tilde{\varphi}}cos\bar{\varphi}\right) \tag{13}$$

For simplicity, we assume $e \simeq 0$ and $\bar{I}_2 \simeq 0$. Therefore, from (1) we deduce that $M_2 \simeq 0$. It must be pointed out that the value of sail inertia is small (almost ten times less than the inertia of the mast) because the sail must be as light as possible. However, it is not actually negligible comparing to the other parameters. Nevertheless, for our goal which is deriving approximate criteria for design, it is permissible to neglect the dynamics of the sail for ease of calculations. The reasonability of this simplification will be validated in Sect. 3.4.

It is also noteworthy that although the dynamics of the sail is neglected, its kinematics, i.e., $\theta(t)$, affects the aerodynamic forces via the effect of angle of attack on C_{D} and C_{L} (see Eqs. (8) and (9) and Sect. 3.1).

Considering $\varphi = \tilde{\varphi} + \bar{\varphi}$ and substituting (12) and (13) and $M_2 = 0$ in (2) and (5), and linearizing around $\bar{\varphi}$, we have

$$\begin{aligned}&\left(\bar{I}_1 + m_1 r^2 + m_2 l^2\right)\ddot{\tilde{\varphi}} + \rho_{\text{air}}Al^2U\left(C_{\mathrm{D}}\cos\bar{\varphi} + C_{\mathrm{L}}\sin\bar{\varphi}\right)\cos\bar{\varphi}\dot{\tilde{\varphi}} \\ &+ \left[K_1 - g\cos\bar{\varphi}\left(m_1 r + m_2 l\right) + \frac{1}{2}\rho_{\text{air}}AlU^2\left(C_{\mathrm{D}}\sin\bar{\varphi} - C_{\mathrm{L}}\cos\bar{\varphi}\right)\right]\tilde{\varphi} \\ &= \frac{1}{2}\rho_{air}AlU^2\left(C_{\mathrm{D}}\cos\bar{\varphi} + C_{\mathrm{L}}\sin\bar{\varphi}\right) + g\sin\bar{\varphi}\left(m_1 r + m_2 l\right) - K_1\bar{\varphi},\end{aligned} \tag{14}$$

and

$$
\begin{aligned}
&\left(\bar{I}_1 + m_1 r^2 + m_2 l^2 + J\right)\ddot{\tilde{\varphi}} \\
&\quad + \rho_{\text{air}} A l^2 U \left(C_{\text{D}} \cos\bar{\varphi} + C_{\text{L}} \sin\bar{\varphi}\right) \cos\bar{\varphi}\dot{\tilde{\varphi}} \\
&\quad + \left[K_1 - g\cos\bar{\varphi}\left(m_1 r + m_2 l\right)\right. \\
&\quad \left. + \frac{1}{2}\rho_{\text{air}} A l U^2 \left(C_D \sin\bar{\varphi} - C_L \cos\bar{\varphi}\right)\right]\tilde{\varphi} \\
&\quad = \frac{1}{2}\rho_{\text{air}} A l U^2 \left(C_D \cos\bar{\varphi} + C_L \sin\bar{\varphi}\right) \\
&\qquad + g\sin\bar{\varphi}\left(m_1 r + m_2 l\right) - K_1\bar{\varphi} + T_{\text{resistive}},
\end{aligned} \tag{15}
$$

where $C_{\text{D}} = C_{\text{D}}(\theta \cdot \text{AR})$ and $C_{\text{L}} = C_{\text{L}}(\theta \cdot AR)$. Let AR = 1 and be constant, then $C_{\text{D}} = C_{\text{D}}(\theta)$ and $C_{\text{L}} = C_{\text{L}}(\theta)$. Equation (14) is the linearized governing equation for the decoupled motion of the mast, and Eq. (15) is the linearized equation of motion for the motion of the mast coupled with flywheel.

Equations (3) and (15) are still nonlinear due to the dry friction torque, $T_{\text{resistive}}$. To remove this nonlinearity, we have to distinguish the sticking and sliding modes according to their conditions and solve the equations of motion separately. Also, we have to consider the rectified rotation of flywheel due to the ratchet mechanism. This will help us with omitting the sign function in (4) and (6).

For the equations of motion to behave linearly, we have to assume the sail to switch between vertical orientation and a small deviation from vertical direction, say δ. This will cause the amplitude of oscillation of mast to remain in the linear margin, because of the small ripple in the aerodynamic force. But the equilibrium state is not necessarily small.

It must be noted that the beginning of the coupled phase (collision) and decoupled phase (separation) are conditional and depends on the values of mast and flywheel angular velocities (see Sect. 2.1), i.e., for $\dot{\varphi} < \dot{\beta}$, the dynamics of the system is decoupled (Eqs. (2) and (3)), and for $\dot{\varphi} = \dot{\beta}$, the system becomes coupled (Eq. (5)). However, in our reduced and simplified model of the system, because of the difficulty in finding the collision and separation moments of mast and flywheel, we tune the parameters of the turbine in a way that coupled phase lies completely in the forward stroke, when the sail is vertical, and the decoupled phase lies in the returning stroke, when the sail is at the small angle δ.

Obviously, the above setup is a specific among many configurations of this turbine and does not represent all aspects of its dynamics. However, this setup simplifies dynamics of the turbine to some extent and makes it possible to derive considered design criteria.

3 Results and Discussions

In order to study the dynamics of the proposed turbine and calculate its power and efficiency, a MATLAB code is generated. A Runge–Kutta algorithm is utilized to solve the equations of motion numerically.

3.1 The Benchmark Parameters of the Turbine

Table 1 contains a set of benchmark parameters selected for the turbine.

The values of drag and lift coefficients are extracted from (Ortiz et al. 2015), for AR = 1.

The parameters are fed to the generated code according to Table 1. The results of the simulation are illustrated in Figs. 2 and 3. The transient part of the response is not shown in both graphs.

The benchmark parameters are set in a way that the amplitude of oscillations of the mast becomes small, so the linearization could be plausible. Furthermore, these parameters are selected in a way that the decoupled and coupled phases of motion can be readily solved in closed form.

As it is obvious in Figs. 2 and 3, each phase of motion (coupled and decoupled) begins when $\varphi = 0$ and $\dot{\varphi} = 0$. This has been maintained by tuning the turbine parameters. This condition is very helpful for the ease of solving the linearized equations of motion and finding the closed answers.

Sticking of the flywheel to the dynamometer belt due to dry friction happens when the flywheel velocity becomes and remains zero (See Fig. 3); otherwise, the flywheel slips on the belt.

3.2 Closed Solution for the Linearized Equations of Motion

Here the turbine response is calculated for only one period of the sail oscillations, considering the transient part of the response have been vanished and the limit cycle of response has been formed.

First of all, the equilibrium angle of decoupled phase of motion is determined. The parameters are set in a way that during the whole decoupled phase $\theta = \delta$.

Letting $\ddot{\tilde{\varphi}} = 0$, $\dot{\tilde{\varphi}} = 0$, and $\tilde{\varphi} = 0$ in (14), We have:

$$
\begin{aligned}
&\frac{1}{2}\rho_{\text{air}} A l \left[C_D(\delta)\cos\bar{\varphi} + C_L(\delta)\sin\bar{\varphi}\right] U^2 \\
&\quad + g\sin\bar{\varphi}\left(m_1 r + m_2 l\right) - K_1\bar{\varphi} = 0 \quad \text{for } 0 \le t \le \frac{T}{2},
\end{aligned} \tag{16}
$$

where T is the sail switching period. Substituting the parameters in (16), we get:

$$
4.4719\cos\bar{\varphi} + 18.4441\sin\bar{\varphi} - 40\bar{\varphi} = 0. \tag{17}
$$

The numerical solution of (17) gives $\bar{\varphi} = 0.2021$rad. Substituting $\bar{\varphi}$ in (14), we have:

$$
1.3333\ddot{\tilde{\varphi}} + 9.6664\dot{\tilde{\varphi}} + 10.5143\tilde{\varphi} = 0. \tag{18}
$$

Solving (18) for the initial conditions $\tilde{\varphi}(0) = a$ and $\dot{\tilde{\varphi}}(0) = 0$, we have:

Table 1 Benchmark parameters of turbine

Parameter	Name	Value	Unit
Mast inertia	$\bar{I}_1$	0.1333	kg m^2
Sail inertia	$\bar{I}_2$	0.0167	kg m^2
Mast mass	m_1	0.4	kg
Sail mass	m_2	0.2	kg
Length of mast	l	2	m
Sail height	b	1	m
Sail width	a	2	m
Position of COG of mast from its axis of rotation	r	1	m
Sail area	A	2	m^2
Angular deviation of sail	δ	$\pi/6$	rad
Air density	ρ_{air}	1.2250	kg/m^3
Gravitational acceleration	g	9.80655	m/s^2
Wind speed	U	1	m/s
Rotational spring constant	K_1	20	N m/rad
Sail switching period	T	10	s
Inertia of flywheel	J	10	kg m^2
Static friction torque between dynamometer belt and flywheel	$T_{\text{static friction}}$	0.1	N m
Kinetic friction torque between dynamometer belt and flywheel	$T_{\text{kinetic friction}}$	0.1	N m
Drag coefficient at $\theta = \delta$	$C_{\text{D}}(\delta)$	0.9126	
Drag coefficient at $\theta = 0$	$C_{\text{D}}(0)$	1.1279	
Lift coefficient at $\theta = \delta$	$C_{\text{L}}(\delta)$	0.56195	
Lift coefficient at $\theta = 0$	$C_{\text{L}}(0)$	0.02832	

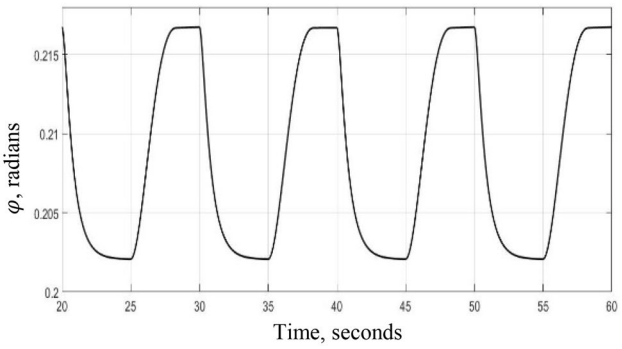

Fig. 2 Time variation of mast angle (results of the numerical simulation by the generated code)

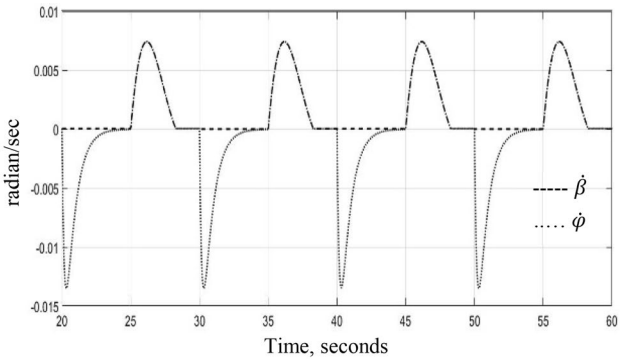

Fig. 3 Time variation of mast and flywheel angular velocity (results of the numerical simulation by the generated code)

$$\tilde{\varphi}(t) = 1.2907ae^{-1.3327t} - 0.2907ae^{-5.9172t}, \tag{19}$$

and also:

$$\dot{\tilde{\varphi}}(t) = -1.7201ae^{-1.3327t} + 1.7201ae^{-5.9172t}, \tag{20}$$

where a is the unknown initial angle of the mast for the decoupled phase. This unknown will be calculated using the periodic behavior of the response. (See below.)

At $t = \frac{T}{2} = 5\,\text{s}$, we have $\tilde{\varphi}(5) = 0.001648a$. Because a is a small number, we may consider $\tilde{\varphi}(5) \cong 0$, or $\varphi(5) \cong \bar{\varphi} = 0.2021$ rad. This will be the initial condition for the next coupled phase.

As it is illustrated in Figs. 2 and 3, the benchmarked parameters are selected in a way that during whole coupled phase, it is admissible to consider $\theta = 0$ (see Sect. 3.1). Letting $\ddot{\bar{\varphi}} = 0$, $\dot{\bar{\varphi}} = 0$, and $\bar{\varphi} = 0$ in (15), we have:

$$\frac{1}{2}\rho_{\text{air}}Al\left[C_D(0)\cos\bar{\varphi} + C_L(0)\sin\bar{\varphi}\right]U^2 + g\sin\bar{\varphi}\left(m_1 r + m_2 l\right) - K_1\bar{\varphi} = 0 \quad \text{for } \frac{T}{2} \le t \le T. \tag{21}$$

Substituting the parameters in (21) leads to:

$$5.5267\cos\bar{\varphi} + 15.8293\sin\bar{\varphi} - 40\bar{\varphi} = 0, \tag{22}$$

which gives $\bar{\varphi} = 0.2219$ rad. Substituting this value in (15), we have:

$$11.3333\ddot{\tilde{\varphi}} + 10.5777\dot{\tilde{\varphi}} + 12.6951\tilde{\varphi} = -0.1. \tag{23}$$

Solving (23) for the initial conditions $\tilde{\varphi}(0) = 0.2021 - 0.2219 = -0.019796$ rad, and $\dot{\tilde{\varphi}}(0) = 0$, we get:

$$\tilde{\varphi}(t) = -0.005855e^{-0.4667t}\sin(0.9499t) - 0.01192e^{-0.46666t}\cos(0.9499t) - 0.007877, \tag{24}$$

and

$$\dot{\tilde{\varphi}}(t) = 0.01405e^{-0.4784t}\sin(0.9441t) + 1.4896\times10^{-7}e^{-0.4784t}\cos(0.9441t), \tag{25}$$

for the coupled phase of motion.

During the coupled phase, if the mast and flywheel speed crosses zero, they remain stationary due to the friction torque, unless the pushing torque generated by wind can overcome the static friction torque.

The angular velocity of the coupled mast plus flywheel becomes zero at $t = 3.3072$ s where we have $\tilde{\varphi}(3.3072) = -0.005330$ rad and $\varphi(3.3072) = -0.005330 + 0.2219 = 0.2165$ rad. This means that the mast together with flywheel stick at $t = 3.3072$ s and remain stationary to the end of the coupled phase.

By switching the sail angle from 0 to δ, the decoupled phase begins again. Therefore, the initial conditions for the decoupled phase are $\dot{\tilde{\varphi}} = 0$ and $\tilde{\varphi} = 0.2165 - 0.2021 = 0.01446$ rad. Consequently, $a = 0.01446$. Substituting in (19) and (20), we get:

$$\tilde{\varphi}(t) = 0.01867e^{-1.2907t} - 0.004205e^{-6.1099t}, \tag{26}$$

and

$$\dot{\tilde{\varphi}}(t) = -0.02488e^{-1.2907t} + 0.02488e^{-6.1099t}, \tag{27}$$

for the decoupled phase of motion.

3.3 Cross-validation of the Analytical Solution Versus the Numerical Simulation

Figures 4 and 5 illustrate the comparison between one cycle of oscillation of mast resulting from numerical simulation and the closed form solution of the linearized equations of motion, derived in Sects. 2.3 and 3.2.

As it is evident, a close likelihood is achieved. This permits us to rely on the linearized equations of motion in order to extract parametric relationships and constraints, as approximate criteria for design and analysis of the turbine.

It is obvious that by increasing the amplitude of oscillations of the sail (δ), the amplitude of oscillations of the mast ($\tilde{\varphi}$) will grow up, and the nonlinear terms will become significant and effective. Therefore, deviation of numerical simulation from the linearized analytical solution will be more serious. However, an exact threshold for the plausibility of the linearized approximation is not exactly definable and is arbitrary.

3.4 Some Criteria Exploited from the Linearized Equations of Motion

There are several parametric relationships derivable from the linearized equations of motion.

First of all, the relationship for equilibrium angle is extractable from the linearized equations of motion. In this work, the sail is considered to switch instantaneously between the vertical orientation and a small deviation from the vertical direction. If the sail oscillates continuously, say,

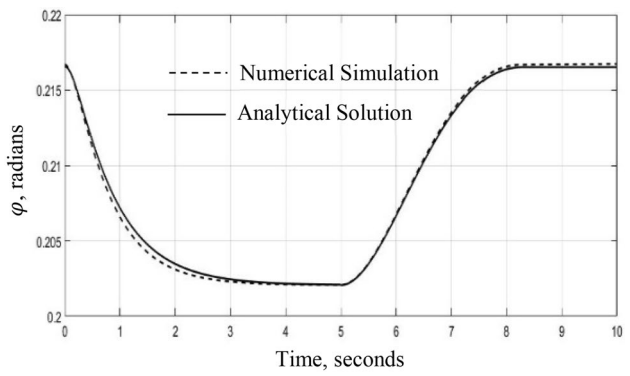

Fig. 4 Time variation of mast angle for one period of oscillations from numerical simulation and analytical solution

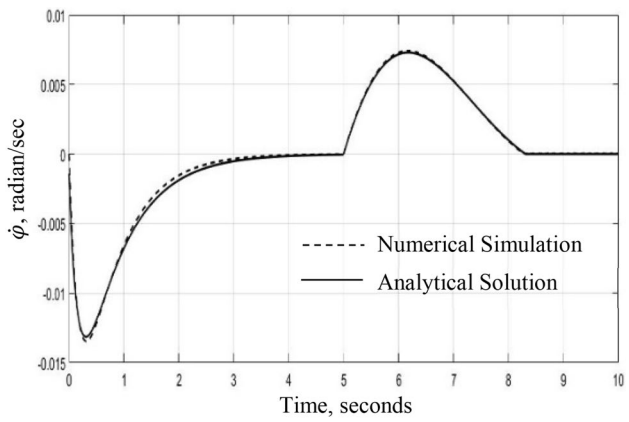

Fig. 5 Time variation of mast angular velocity for one period of oscillations from numerical simulation and analytical solution

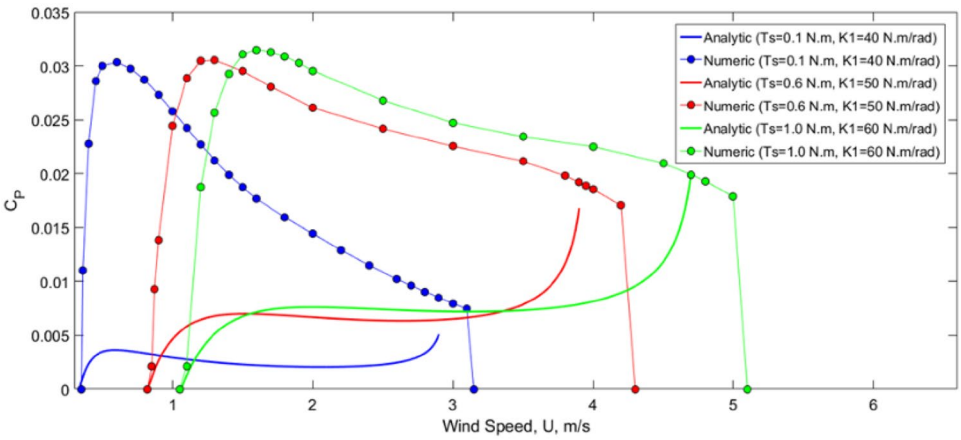

Fig. 6 Comparison of C_P versus wind speed from analytical relationship (Eq. 31) and numerical data for benchmarked turbine for three combinations of resistive torque and spring constant

harmonically, we have to integrate the equation of motion over one period of oscillation to find $\bar{\varphi}$.

Letting $\ddot{\tilde{\varphi}} = 0$, $\dot{\tilde{\varphi}} = 0$, and $\tilde{\varphi} = 0$ in (14) or (15), and integrating over one period of sail oscillation, we get:

$$\frac{1}{2}\rho_{\text{air}} AlU^2 \left[\cos\bar{\varphi}\int_0^T C_{\text{D}}(\theta)\mathrm{d}t + \sin\bar{\varphi}\int_0^T C_{\text{L}}(\theta)\mathrm{d}t\right] - I_2\int_0^T \ddot{\theta}(t)\mathrm{d}t + g\left(m_1 r + m_2 l\right)T\sin\bar{\varphi} - T\bar{\varphi} = 0. \tag{28}$$

Another useful criterion for designing the turbine is the stability criterion. For the turbine to be stable, it is desirable that equivalent stiffness and equivalent damping of the linearized equation both be positive. From Eqs. 14 or 15, we deduce:

$$K_1 - g\cos\bar{\varphi}\left(m_1 r + m_2 l\right) + \frac{1}{2}\rho_{\text{air}} Al\left[C_{\text{D}}(\theta)\sin\bar{\varphi} - C_{\text{L}}(\theta)\cos\bar{\varphi}\right]U^2 > 0, \tag{29}$$

and

$$\rho_{\text{air}} Al^2 U\left[C_{\text{D}}(\theta)\cos\bar{\varphi} + C_{\text{L}}(\theta)\sin\bar{\varphi}\right]\cos\bar{\varphi} \geq 0, \tag{30}$$

depending on the worst values for $C_{\text{D}}(\theta)$ and $C_{\text{L}}(\theta)$.

To investigate the significance of the method utilized in this work, we consider $\theta_{\text{coupled}} = 60°$ and $\theta_{\text{decoupled}} = 90°$, and for further simplification, we assume $\bar{\varphi}$ is small (albeit not zero). By solving the steady-state response of the benchmarked turbine, the C_P of the turbine will be derived as

$$C_P = \frac{P}{\frac{1}{2}\rho_{\text{air}} AU^3} = \frac{2T_s\left(\rho_{\text{air}} C_D AlU^2 - 2T_s\right)}{\lambda\pi\rho_{\text{air}} AU^3\sqrt{I+J}\sqrt{K_1 - g\left(m_1 r + m_2 l\right) + \frac{1}{2}\rho_{\text{air}} C_{\text{L}} AlU^2}}, \tag{31}$$

where C_D and C_L are drag and lift coefficients of coupled phase, respectively, $I = \bar{I}_1 + m_1 r^2 + m_2 l^2$, $\lambda = \frac{J}{I}$, and $T_{\text{s}} = T_{\text{static friction}}$. Figure 6 compares (31) with numerical results generated by the code for the benchmark turbine. As it is obvious from the figure, the analytical formula forecasts the cut-in and cut-out wind speeds, and the speed at which C_P is maximum. It is noteworthy that the cut-out speed is the verge of instability of the turbine. However, the value of C_P calculated by (31) differs significantly with the numerical results. A proper correction factor can be obtained experimentally to scale the analytical value.

4 Conclusion

In this work, a noble oscillatory wind turbine is studied. The reduced approximated equations for different phases of motion of the turbine have been linearized, and the closed solutions of these equations have been compared with numerical results of a generated computer code.

The comparison shows good likelihood between analytical and numerical methods, which permits some parametric relationships and criteria extracted from the linearized equations of motion to be utilized as approximate rules of thumb in design and analysis of the wind turbine.

Among these relationships are some important ones derived from the linearized equations of motion in this work: the equation of equilibrium angle of mast, and the criteria of stability of turbine.

To validate whether this method is significant or not, an approximate formula for C_P is derived and compared with the numerical results.

As further work, more approximate parametric criteria may be extracted from the linearized equations of motion, especially for optimization purposes. Also, it seems better to check the validity of the linearized equations of motion for more sets of turbine parameters.

The experimental validation of the linearized equations and the approximate criteria extracted from these equations are left as a further work, after fabricating a prototype of the turbine.

Acknowledgements I would like to thank Dr. Mojtaba Mahzoon, from Shiraz University, School of Mechanical Engineering, for his helpful comments and directions on linearization of dynamical systems.

References

Anderson JM, Streitlien K, Barrett DS, Triantafyllou MS (1998) Oscillating foils of high propulsive efficiency. J Fluid Mech 360:41–72

Armstrong-Helouvry Brian, Dupont Pierre, Wit Carlos Canudas De (1994) A survey of models, analysis tools and compensation methods for the control of machines with friction. Automatica 30(7):1083–1138

Arrowsmith DK, Place CM (1995) Dynamical systems, differential equations, maps and chaotic behavior. Chapman and Hall Mathematics, London

AWEA (2017) AWEA 2016 fourth quarter market report. American Wind Energy Association. Retrieved 9 February 2017

Bakhshandeh Rostami A, Armandei M (2017) Renewable energy harvesting by vortex-induced motions: review and benchmarking of technologies. Renew Sustain Energy Rev 70:193–214

EWEA (2017) Wind in power: 2016 European statistics. European Wind Energy Association. February 2017

Kinsey T, Dumas G (2008) Parametric study of an oscillating airfoil in a power-extraction regime. AIAA J 46:1318–1330

Lan CE (1979) The unsteady quasi-vortex-lattice method with applications to animal propulsion. J Fluid Mech 93(4):747–765

Liu N, Peng Y, Liang Y, Lu X (2012) Flow over a traveling wavy foil with a passively flapping flat plate. Phys Rev E 85:056316

McKinney W, DeLaurier J (1981) Wingmill: an oscillating-wing windmill. J Energy 5:109–115

Ortiz Xavier, Rival David, Wood David (2015) Forces and moments on flat plates of small aspect ratio with application to PV wind loads and small wind turbine blades. Energies 8:2438–2453

Pennestri E, Rossi V, Salvini P, Valentini PP (2016) Review and comparison of dry friction force models. Nonlinear Dyn 83:1785–1801

Perko L (1991) Differential equations and dynamical systems. Springer, New York

Platzer MF, Jones KD, Young J, Lai JCS (2008) Flapping-wing aerodynamics: progress and challenges. AIAA J 46(9):2136–2149

Triantafyllou MS, Triantafyllou GS, Yue DKP (2000) Hydrodynamics of fishlike swimming. Annu Rev Fluid Mech 32:33–53

Xiao Q, Zhu Q (2014) A review on flow energy harvesters based on flapping foils. J Fluids Struct 46:174–191

Young J, Lai JCS, Platzer MF (2014) A review of progress and challenges in flapping foil power generation. Prog Aerosp Sci 67:2–28